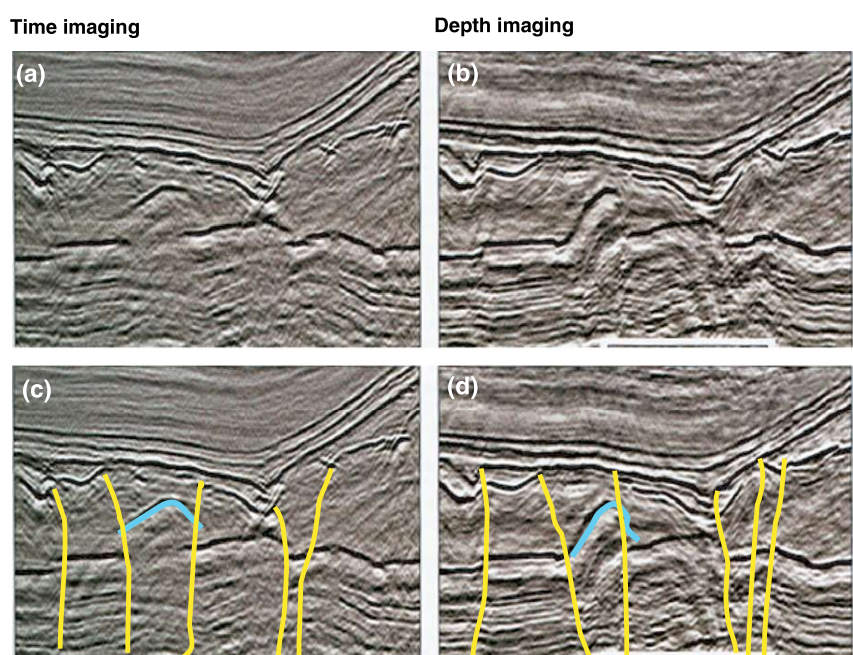


FIGURE 11.45. A complex Rotliegende structure revealed by migration, especially depth migration. Diagrams (a) and (c) show the time-migration section, and (b) and (d) show the depth migration. Notice that (a) and (c) are identical sections; we have added only an interpretation of the salt bodies to (c). A disrupted interval in the time-migrated section is difficult to interpret. In the depth-migrated image, this becomes identifiable as a pop-up of the Rotliegende strata. The pop-up is indicated by light blue lines, and faults are indicated by solid yellow lines. (Adapted from Christie et al., 2001.)



base. Instead of being flexed into an anticlinal structure, strata appear to be truncated along the flanks of the salt hourglass, because the velocity pull-up of the top-salt overhang is not compensated for in time migration.

Figure 11.45 shows an example from the Dutch sector of the North Sea. The feature that is difficult to interpret in the time-migrated section becomes identifiable as a “pop-up” of the Rotliegende Series in the properly depth-migrated image. What appears to be an isolated, discontinuous reflection in time migration can be seen in the depth-migrated section to be an abrupt pop-up with nearly vertical sides. The complex structure overlying the pop-up, combined with the steeply dipping flanks of the pop-up, make this problem difficult to solve with time migration but completely tractable with depth migration. Compare the time imaging with the depth imaging, and notice the differences in the interpretations of faults.

MODELS FOR ESTIMATING BACKGROUND VELOCITY

Linking the Imaging Requirements with the Background-velocity Estimation

The imaging algorithms described in the previous sections depend on an accurate knowledge of the background-velocity model for their successful application. In other words, we need to know at least some

parts of the model of the subsurface in order to reconstruct the “entire” model. This requirement is known as the paradox of seismic imaging. As we described in the first section of this chapter, this paradox of our current imaging techniques is because of the Born-like approximations that are made implicitly or explicitly in our current imaging techniques.

Fortunately, the requirements of an accurate background-velocity model for successful imaging can be used to estimate the background model if the geology is not too complex. As we can see in the simple example of data that have a single reflected event in Figure 11.46, imaging of the reflector associated with these events is quite sensitive to velocity. As we discussed in the previous section, we need to correct for the traveltimes variations with offsets (moveout) and perform an intelligent stack. As Figure 11.47 illustrates, with a data set containing evidence of three events, the correct background velocity corresponds to the maximum-amplitude-moveout correction and stack. This idea essentially amounts to “focusing” the seismic traces, so that a large response is obtained. When the traces are properly lined up (i.e., properly moveout-corrected), then the sum of traces will be maximized. This idea is similar to the focusing actions of a lens or of a parabolic reflector for plane waves.

Thus, the basic idea for reconstructing the background velocity is to image our data with various velocity models and to select the model that produces focused images of the subsurface. The two basic components of

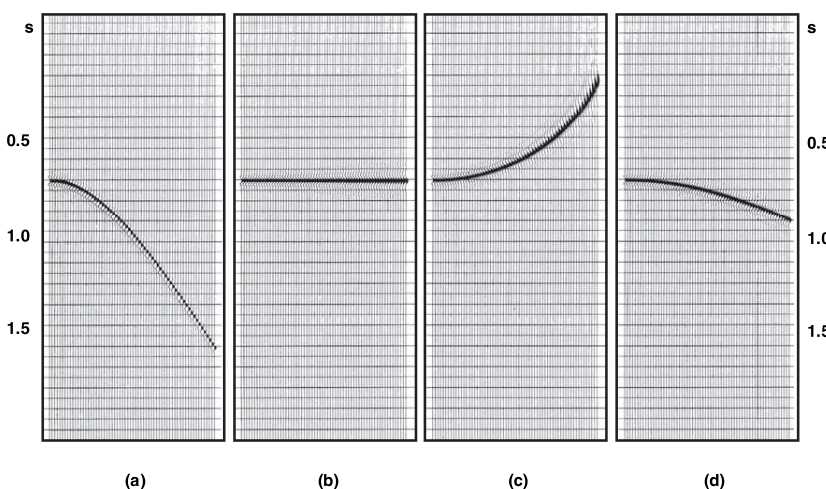


FIGURE 11.46. (a) CMP gather containing a single event with a moveout velocity of 2264 m/s. (b) NMO-corrected gather using the appropriate moveout velocity. (c) Overcorrection because the velocity (2000 m/s) used was too low. (d) Under-correction because the velocity (2500 m/s) used was too high. (Adapted from Yilmaz, 1987.)

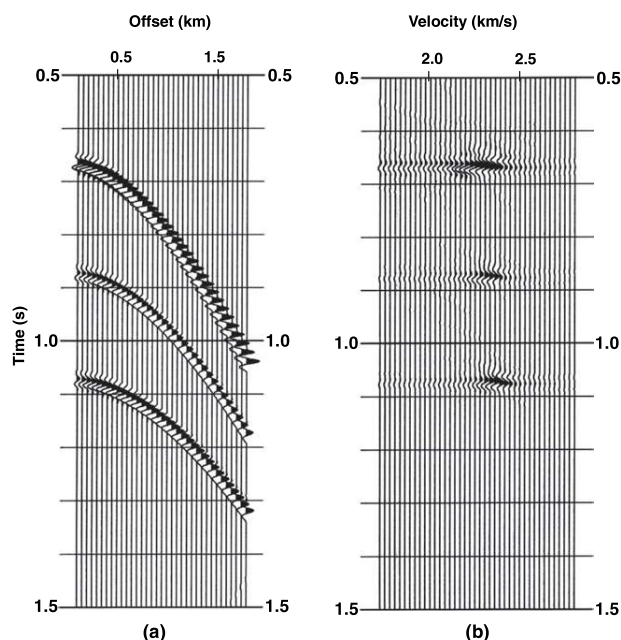


FIGURE 11.47. (a) A CMP gather that contains evidence of three reflection events. (b) The result of a scan over different velocity models. Notice that the maximal amplitudes correspond to the optimal velocity model.

this approach to estimating the background are (1) the tool used for imaging the data and (2) the criteria for determining the best velocity model. In the examples in Figures 11.46 and 11.47, because of the simplicity of the problem, the imaging tool was NMO-plus-stack, and the criterion for selecting the correct velocity was the amplitude of stack results. Another quantity used is semblance (see Box 11.9).

Essentially, we have two types of imaging techniques: time imaging and depth imaging. The background-velocity requirement of time imaging is the

rms velocity, whereas that of depth imaging is the actual velocity (also called the interval velocity). Unfortunately, implementing the idea of focusing and defocusing, described above, differs significantly between time imaging and depth imaging. Because we violate Snell's law in time imaging, the concept of focusing and defocusing can be applied to each event in the data, independently of the other events. The good news is that we can scan all the events simultaneously for estimating the rms velocities, by performing a number of migrations over a range of constant-velocity models or even through a set of heterogeneous-velocity models. Figure 11.47 illustrates an example in which three events are scanned simultaneously.

In depth imaging, we do not violate Snell's law, because we do not use a constant background velocity. Therefore, to successfully depth-image an event at a given depth, we need to know the actual velocity variations above that depth. Thus, we have to scan for the actual velocity, layer by layer, starting from the surface. Alternatively, we can scan over a set of heterogeneous-velocity models, to recover the background velocity. We will discuss, in more detail, some techniques for recovering the interval velocity for depth imaging. However, we will start with velocity estimation for time imaging.

Velocity Spectrum

The plot in Figure 11.47 is called a velocity spectrum. The quantity represented in this figure is the amplitude of the stacks of NMO-corrected CMP gathers. Another quantity used in velocity-spectrum calculations is the semblance defined in Box 11.9. Actually,

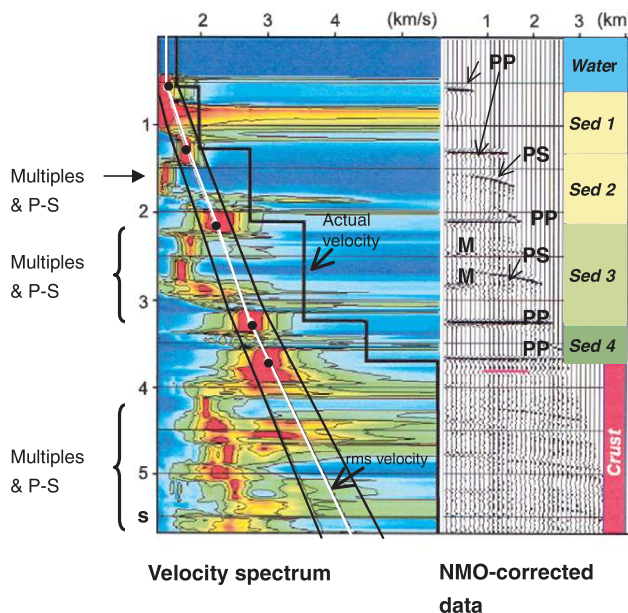


FIGURE 11.48. Velocity semblance plot. Velocity analysis of finite-difference modeled data. The model is superimposed on the CMP gather. Note how the velocity analysis shows a good fit between the semblance peaks (red) and the theoretically computed rms velocities (black dots superimposed on a white curve). PP indicates P-to-P reflection, PS and P-S indicate P-to-S reflections.

the velocity spectra commonly are displayed on the basis of semblance, as Figure 11.48 shows. We can see that the semblance plot in Figure 11.48 has the better standout of strong reflections. Data used in this plot and in the following plot, in Figure 11.49, are synthetic data computed by the finite-difference technique. The models used to generate the data are elastic, although only the P-wave velocity models are shown in Figures 11.48 and 11.49, because our discussion will focus primarily on P-P reflections. In Figure 11.49, these strong reflections are shown in red. We can easily pick them based on the fact that the rms velocity generally increases with time or depth. Moreover, this pick fits well with the theoretically calculated rms velocities (white curve).

Note that we can select from various alternative red peaks in the semblance plot. Some of these peaks are multiple reflections that are not taken in the calculation of rms velocities. The fact that rms velocity generally increases allows us to avoid picking the red peaks that correspond to multiple reflections.

Various scenarios exist in which picking the correct velocity in the semblance can be a daunting task.

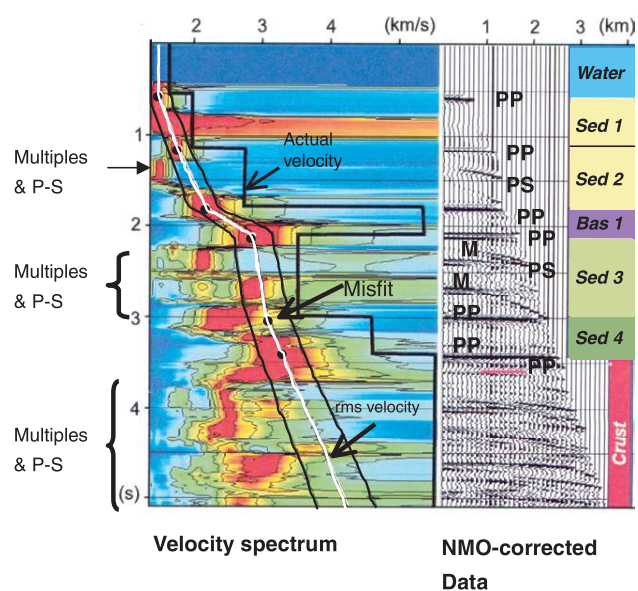


FIGURE 11.49. Velocity semblance plot. Velocity analysis of synthetic data corresponding to a model of the subsurface with one high-velocity basalt layer. The model is superimposed on the CMP gather. Note the significant misfit between theoretically computed rms velocities (black dots superimposed on a white curve) and the semblance peaks (red). This misfit results from the presence of the basalt layer. PP indicates P-to-P reflection, PS and P-S indicate P-to-S reflections.

Figure 11.49, which corresponds to a simple model of the subsurface, shows one such example. This model includes one high-velocity basalt layer. In contrast to Figure 11.48, there is now a large misfit between the theoretically computed rms velocity and the red peaks of the semblance plot at around 3 s. This misfit results from the fact that traveltimes variations are non-hyperbolic, whereas our velocity spectra are computed on the basis of NMO-plus-stack, which assumes that traveltimes variations with offsets follow a hyperbolic moveout. In other words, this misfit occurs because of the limitations of our imaging tools and the limitations of the focusing and defocusing idea. In the next subsections, we discuss an extension of this focusing and defocusing idea for sophisticated imaging tools.

The semblance plot in Figure 11.49 also shows high-amplitude events arriving at greater traveltimes than was the case in the semblance plot in Figure 11.48. These are clearly not primary, but are instead various multiples and converted waves. This observation illustrates the difficulty of distinguishing real primaries from multiples generated above the basalt.

Velocity-migration Analysis

The method of estimating rms velocity described in Figures 11.48 and 11.49 is based on NMO-plus-stack. This method makes sense only if the reflectors are horizontally flat and if traveltime variations with offsets follow a hyperbolic moveout. For large dips, the error in the velocity model can be large.

An alternative method is to replace NMO-plus-stack with a prestack time-migration algorithm like the one in equation (11.202). Many constant-velocity migrations are performed, for velocities between V_{\min} and V_{\max} , with a step of ΔV . In the example displayed in Figure 11.50, we take $V_{\min} = 2050$ m/s and $V_{\max} = 3350$ m/s. ΔV is taken to be equal to 50 m/s. Because of limited space, migration results in Figure 11.50 are shown only every 200 m/s. Still, we can clearly see the events focusing as we reach the correct velocity and then defocusing as soon as we move away from the correct velocity. For instance, events A and B are best migrated with a 2050 m/s velocity. However, event C is best migrated with a 3050 m/s velocity. This example confirms that any imaging algorithms can be used for velocity estimation. The velocity estimation based on prestack time migration is known as velocity-migration analysis.

Note that the final migration image can be formed from scans in Figure 11.50 by merging parts of each constant-velocity migration so that every part of the final image section has the correct effective velocity.

Velocity Building

Before depth imaging can be done, an accurate velocity model in depth must be created, or, alternatively, the depth imaging and accurate velocity model in depth must be obtained simultaneously. First, the velocity model is considered to be a series of velocity functions. The process of constructing these functions generally is called velocity model building.

Model building is an iterative process, most commonly done layer by layer, whereby new information is constantly fed into the model to refine the final result. As in any iterative process, the first step is to create an initial-velocity model.

Creating an initial-velocity model. Two types of velocities commonly are used in creating an initial-velocity model from seismic data: rms velocities (from

time imaging) and interval velocities. The rms velocities are picked from the semblance plots of CMP gathers and then converted to interval velocities, using, for instance, Dix's formula in Box 3.3. These interval velocities are used to construct a starting model.

As we discussed in the section titled "Key Assumptions of our Example of an Inverse Problem," smoothing the interval velocities is critical, because an unsmoothed velocity field may contain abrupt changes that can introduce a false structure on the final depth-migrated section.

Iterative process. The first step is to run the prestack depth migration (PSDM) using the initial-velocity model. The next step is the process of residual-moveout (RMO) analysis. RMO is the amount of residual moveout observed on the CRP (common-reflection-point) gathers. After RMO analysis, we then modify the velocity so that RMO is minimized on the CRP gathers.

There are two basic ways to attain a final-velocity model effectively: the layer-by-layer approach and the global scheme. The layer-by-layer approach involves working on one layer at a time, starting with the top horizon. Each layer will have geophysical and geologic constraints. As the top layer is finalized and its velocity converges to a "true" value, the processor "locks" that layer into place so that no additional velocity changes are made to it. Once this is done, the same iterative process is performed on the next layer down. This process is repeated until every layer has been processed individually and the velocity model is complete. Commonly, this technique is used in areas with complex geologic structure (Figure 11.51).

The global approach involves working with the entire model. Each layer will still have its geophysical and geological constraints. This approach differs in that the entire model is modified with each iteration, until the entire model converges within a certain tolerance (Figure 11.52).

IMAGING RECEIVER GHOSTS OF PRIMARIES

The present inversion and migration algorithms, like the ones described previously, are designed for imaging primary reflections. For the future, we anticipate that inversion and migration will also be applied to multiples, receiver ghosts of primaries, downgoing

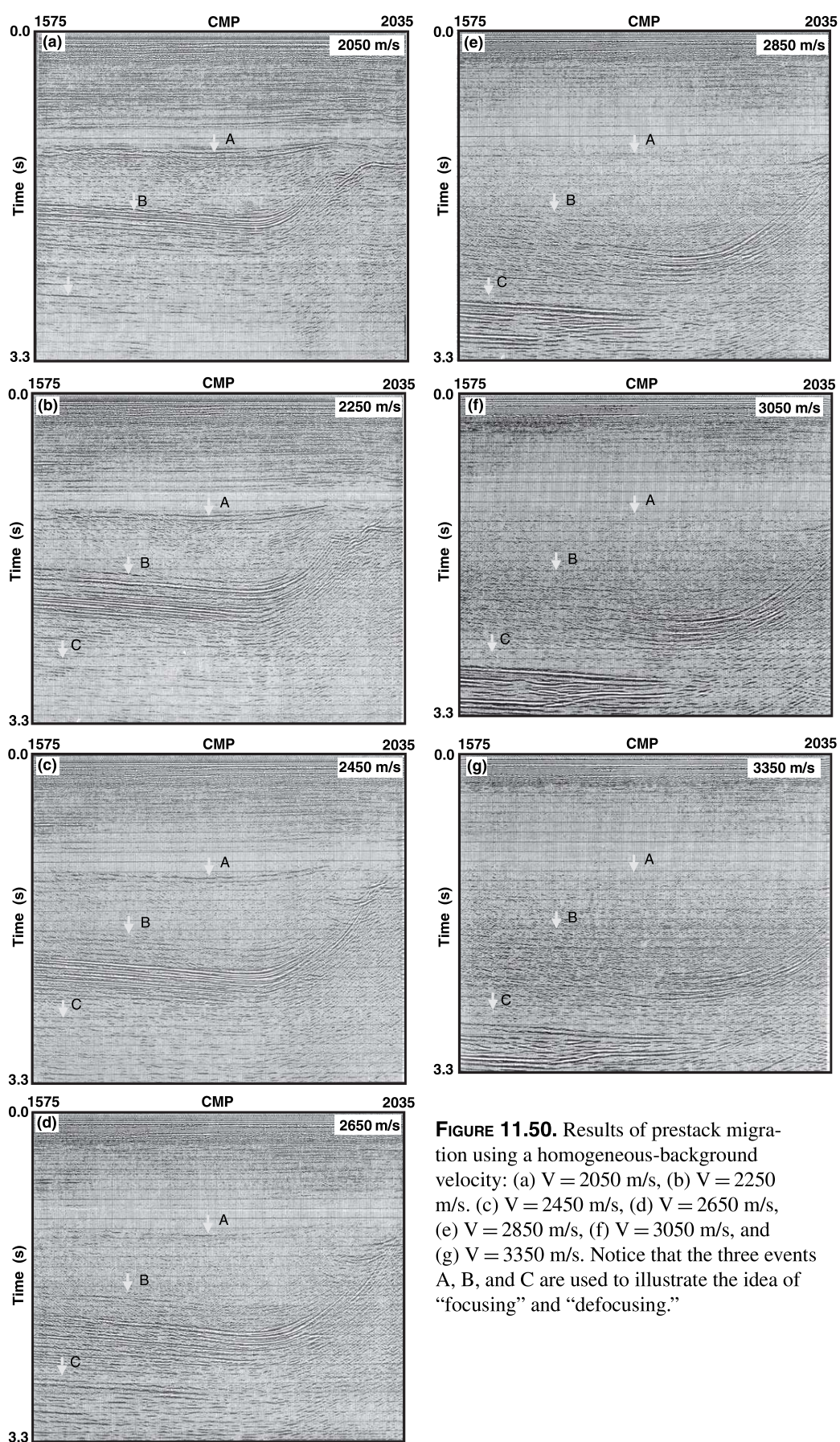
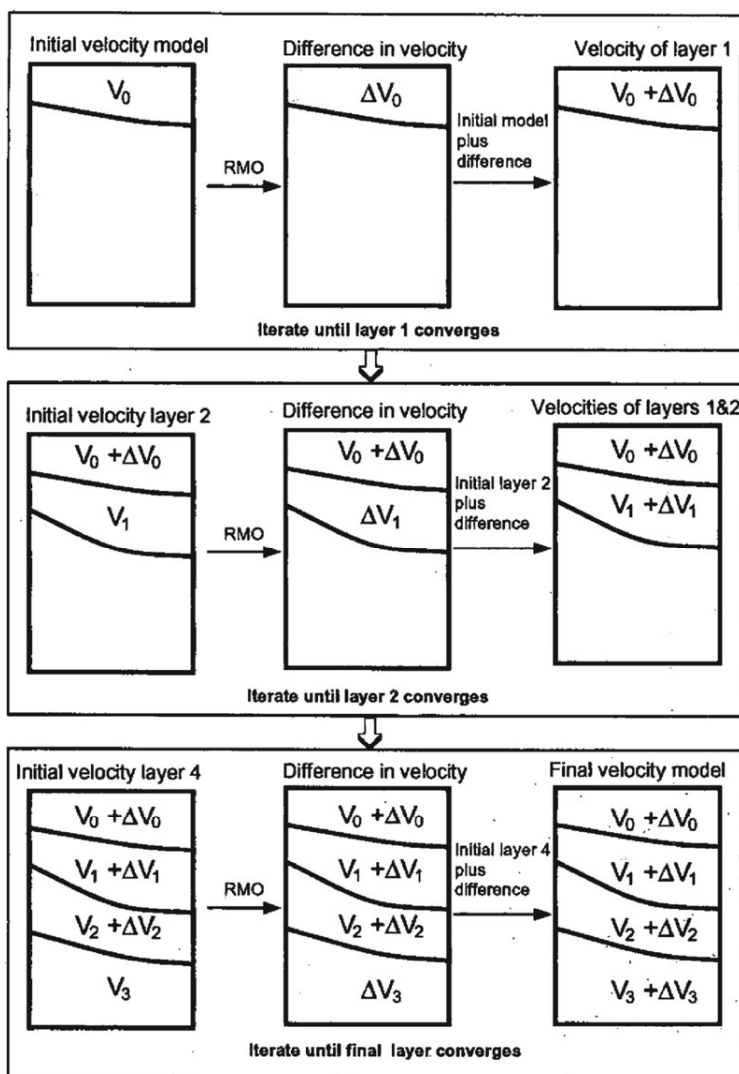


FIGURE 11.50. Results of prestack migration using a homogeneous-background velocity: (a) $V = 2050$ m/s, (b) $V = 2250$ m/s, (c) $V = 2450$ m/s, (d) $V = 2650$ m/s, (e) $V = 2850$ m/s, (f) $V = 3050$ m/s, and (g) $V = 3350$ m/s. Notice that the three events A, B, and C are used to illustrate the idea of “focusing” and “defocusing.”



V_0 , V_1 , V_2 , and V_3 are velocities. RMO: residual moveout.
 ΔV_0 , ΔV_1 , ΔV_2 , and ΔV_3 are velocities of residuals obtained from RMO analysis.

wavefields, and the like — in other words, to some of the seismic energy that is disregarded by the present processing algorithms. Actually, this type of imaging is already happening in the processing of vertical cable (VC) data, in which receiver ghosts of primaries are imaged in addition to the primaries themselves. The principle obviously applies to OBS data recorded in deep water.

As we discussed in Chapter 7, one of the major differences between VC data and surface seismic data, in particular towed-streamer data, is the nature and use of receiver ghosts. In surface seismic data, the effect of receiver ghosts is negligible, or they (the receiver ghosts of primaries) are generally treated as part of an effective

FIGURE 11.51. Illustration of the steps used in estimating the background-velocity model for depth migration. The method described works layer by layer.

source signature because the receivers are very close to the sea surface. In VC experiments, the problem is quite different; receiver ghosts can be distinct from primaries and multiples, as we illustrated in Chapter 7. Moreover, the early developments of VC-imaging algorithms tend to use receiver ghosts of primaries in addition to primaries themselves, because they allow us to increase the illumination of the subsurface (e.g., Krail, 1994). The basic idea is that the receiver ghosts of primaries improve the coverage of small incident angles, which are not densely covered by primary reflections in VC experiments.

Let us illustrate this point with a numerical example. Figure 11.53 shows a 2D acoustic model (with constant density) and snapshots of the wave propagation through this model. We generated 2D VC synthetic data through this model by use of the finite-difference technique. The VC data include four vertical cables, with each cable consisting of 16 receivers at 25-m intervals, starting at a depth

of 800 m and reaching to 1175 m below sea level. The shot spacing was 50 m, the distance between cables was 1250 m (other distances between cables will be considered later), and the listening time was 6 s.

The imaging results in Figures 11.54 through 11.56 were obtained by prestack depth migration (PSDM), which we described earlier. The exact interval velocities used in the finite-difference modeling, resampled at 50 m, were supplied as the migration velocity model of the PSDM application. The method for generating the Green's functions was based on the Eikonal equation in Box 11.8.

Let us now discuss the imaging results, starting with a comparison of the migrated results of primaries and